Published in final edited form as:
Eur Respir J. 2009 May ; 33(5): 1113–1121. doi:10.1183/09031936.00015108.

Muscarinic receptor subtypes in cilia-driven transport and airway epithelial development

Maike K. Klein[*,1], **Rainer V. Haberberger**[*,†], **Petra Hartmann**[*], **Petra Faulhammer**[*], **Katrin S. Lips**[*], **Benjamin Krain**[*,‡], **Jürgen Wess**[§], **Wolfgang Kummer**[*], and **Peter König**[*,‖,1]

[*]Institut für Anatomie und Zellbiologie and University of Giessen Lung Center, Justus-Liebig-Universität Giessen, Giessen, Germany

[†]Department of Anatomy and Histology, Flinders University, Adelaide, SA, Australia

[‡]Abteilung für Anaesthesie, Operative Intensivmedizin, Schmerztherapie, Justus-Liebig-Universität Giessen, Giessen, Germany

[§]Laboratory of Bioorganic Chemistry, National Institute of Diabetes and Digestive and Kidney Diseases, Bethesda, Maryland, USA

[‖]Institut für Anatomie, Zentrum für Medizinische Struktur- und Zellbiologie, Universität zu Lübeck, Lübeck, Germany

Abstract

Ciliary beating of airway epithelial cells drives the removal of mucus and particles from the airways. Mucociliary transport and possibly airway epithelial development are governed by muscarinic acetylcholine receptors but the precise roles of the subtypes involved are unknown.

This issue was addressed by determining cilia-driven particle transport, ciliary beat frequency, and the composition and ultrastructural morphology of the tracheal epithelium in M1–M5 muscarinic receptor gene-deficient mice.

Knockout of M3 muscarinic receptors prevented an increase in particle transport speed and ciliary beat frequency in response to muscarine. Furthermore, the ATP response after application of muscarine was blunted. Pretreatment with atropine before application of muscarine restored the response to ATP. Additional knockout of the M2 receptor in these mice partially restored the muscarine effect most likely through the M1 receptor and normalized the ATP response. M1, M4, and M5 receptor deficient mice exhibited normal responses to muscarine. None of the investigated mutant mouse strains had any impairment of epithelial cellular structure or composition.

In conclusion, M3 receptors stimulate whereas M2 receptors inhibit cilia-driven particle transport. The M1 receptor increases cilia-driven particle transport if the M3 and M2 receptor are missing. None of the receptors is necessary for epithelial development.

Keywords

cholinergic signal transduction; epithelial development; knockout mice; mucociliary clearance

Please send correspondence to: Peter König, Institut für Anatomie, Zentrum für Medizinische Struktur- und Zellbiologie, Ratzeburger Allee 160, 23538 Lübeck, Germany, Tel.: +49-451-500-4022, Fax: +49-451-500-4034, koenig@anat.uni-luebeck.de.
[1]both authors contributed equally to this study

Introduction

Mucociliary clearance is a primary defense mechanism of the airways against inhaled microorganisms and noxious particles. Ciliated cells propel mucus and particles by the coordinated beating of their cilia. Ciliary beat frequency (CBF) which is generally believed to increase mucociliary transport, can be increased by acetylcholine (ACh) [1, 2]. ACh is the main transmitter of parasympathetic nerve fibers in the airways but it can also be released from the bronchial epithelium and cells of the immune system [3, 4]. It exerts its ciliostimulatory effect via muscarinic receptors (MR) [1, 5].

Five MR subtypes (M1-M5R) have been identified by molecular cloning [6]. Activation of each subtype can lead to different physiological effects based on the specific distribution pattern of each of these receptors and the signaling cascades they are linked to [6–8].

In murine, porcine, and human lung, at least three MR subtypes, M1R, M2R, and M3R are expressed [9–12]. Pharmacological studies suggest that the M1R and M3R subtypes are involved in the regulation of CBF [1, 5]. However, conclusions derived from experiments using pharmacologic inhibitors are limited by the rather small degree of MR subtype selectivity of these agents [8].

In the present study, we used mouse strains with genetic disruptions of the M1R, M2R, M3R, M4R, and M5R genes [8], in order to assess the role of each individual MR in regulating surface particle transport of the tracheal epithelium and on CBF. We also examined the effect of MR deficiency on ATP signaling because ATP is an important epithelial mediator known to regulate CBF and is endogenously released from the airway epithelium [13, 14]. Since MR have also been implied in regulating proliferation and, possibly, differentiation of airway epithelial cells [4, 15], we also determined the epithelial cell type composition and cellular ultrastructure to elucidate whether the lack of specific MR subtypes is associated with specific histological changes that might transmit into impaired mucociliary transport.

Materials and Methods

Animals

The generation of $M1R^{-/--}$, $M2R^{-/-}$, $M3R^{-/-}$, $M4R^{-/-}$, $M5R^{-/-}$, and $M2/3R^{-/-}$ mice has been described previously [16–21].

The $M1R^{-/-}$ and $M3R^{-/-}$ mice and the corresponding wild-type mice that were used for studies examining relative cell frequencies had the following genetic background: 129SvEv (50%) × CF1 (50%). The $M2R^{-/-}$ mice and the corresponding WT mice (M2R+/+ mice) had a slightly different genetic background [20]: 129J1 (50%) × CF1 (50%). For functional studies and for the determination of the number of brush and neuroendocrine cells, knockout mice were used that had been backcrossed for at least ten generations onto the C57BL/6NTac background. C57BL/6NTac mice were used as WT controls. Animals deficient in both the M2R and M3R subtypes ($M2/3R^{-/-}$) and control mice ($M2/3R^{+/+}$) with an equivalent genetic background (129J1 (25%) × 129SvEv (25%) × CF1 (50%)) were generated as previously described [21]. Adult mice of both sexes that were at least 8 weeks old were used for all experiments. All mice were held under specified pathogen-free conditions prior to experiments. All experiments were made in accordance with the German animal protection law.

Real time RT-PCR

The epithelial cells from the tracheae of WT, $M1R^{-/-}$ mice, $M3R^{-/-}$ mice, and $M2/3R^{-/-}$ mice (n = 5 each) were abraded using cotton swabs that were carefully rolled over the epithelial layer, and the total RNA was isolated by using the RNeasy method according to the manufacturer's protocol (Qiagen, Hilden, Germany). Contaminating DNA was degraded using 1 U DNase-I (Invitrogen, Karlsruhe, Germany) per μg of total RNA, and reverse transcription was done for 50 min at 42°C using 200 U Superscript II reverse transcriptase (Invitrogen) per μg of RNA.

Real-time quantitative PCR was performed in an I-Cycler (Bio-Rad, Munich, Germany) using QuantiTec SYBR Green PCR kit (Qiagen). Primer sets for the different MR subtypes and the house keeping gene β2-microglobulin (β2-MG) are given in Supplemental Table 3. The PCR conditions included initial denaturation for 10 min at 95°C followed by 40 cycles of 20 s at 95°C, 20 s 62°C, and 20 s at 72°C. All analyses were done in triplicate. For quantification, the mean cycle thresholds (CT) were calculated and the corresponding CT values of the target gene were subtracted from mean β2-MG-CT according to:

$$\Delta CT = CT_{\text{target gene}} - CT_{\beta 2\text{-MG}}$$

The difference of expression of a target mRNA between two mouse strains was calculated according to:

$$\Delta\Delta CT = \Delta CT_{\text{target gene, strain a}} - \Delta CT_{\text{target gene, strain b}}$$

The PCR products were analyzed by electrophoresis on a 2% TRIS-acetate-EDTA agarose gel.

Evaluation of epithelial composition and morphology, and immunohistochemistry for the M2R

For electron microscopy and determination of cell numbers, $M1R^{-/-}$, $M2R^{-/-}$, $M3R^{-/-}$, and their respective WT mice (n = 5 each) were killed by an overdose of isoflurane and perfusion-fixed using a solution containing 2.5% polyvinylpyrrolidone (Sigma) and 0.5% procainamide•HCl (Sigma) [22] to remove blood, followed by fixative containing 100 ml 1.5% glutardialdehyde and 2% paraformaldehyde in 0.1 M phosphate buffer (PB), pH 7.4. The trachea was removed, dissected into a laryngeal and a thoracic part and stored for 1 h in fixative. Then, the tissue was stained en block using OsO_4 and uranyle acetate, dehydrated in increasing alcohol concentrations and embedded in Epon. Semithin sections (1 μm) of whole tracheal cross sections were cut using an Ultracut E ultramicrotome (Leica, Bensheim, Germany) mounted on glass slides, stained with Rüdeberg stain and coverslipped with Eukitt (Fluka, Buchs, Germany).

To quantify the relative numbers of epithelial cells, the sections were viewed using a bright field microscope (Olympus BX60, Hamburg, Germany) equipped with a 60× oil immersion objective lens. The epithelium was grouped in three regions, according to its underlying tissue: cartilage, tracheal muscle, and the ligament. Two hundred cells for each region (a cell was counted if its nucleus was visible) were examined and the portion of ciliated, non-ciliated, and basal cells was determined.

Of the same specimen, ultrathin sections were cut and counterstained with lead citrate. They were evaluated for morphologic changes in epithelial cells using a transmission electron microscope (EM 906, Leo, Wörrstadt, Germany).

To determine if deficiency in muscarinic receptors influences the number of brush cells or neuroendocrine cells, $M1R^{-/-}$, $M2R^{-/-}$, $M3R^{-/-}$, and WT mice (n = 5 each) were perfusion-fixed as described above using 4% paraformaldehyde in 0.1 M phosphate buffer (PB) as

fixative. Tracheas were removed, dissected into a laryngeal and a thoracic part, washed, cryoprotected with 18% sucrose, oriented to allow cutting of cross sections and snap-frozen in liquid nitrogen. Ten μm thick frozen sections were cut and incubated using either rabbit polyclonal antibody against protein gene product (PGP) 9.5 (1:10,000, Biotrend, Cologne, Germany) to label neuroendocrine cells or rabbit polyclonal antibody against villin [23] to stain brush cells. The following secondary reagents were used: Cy3-conjugated donkey anti-mouse IgG antibody and Cy3-conjugated donkey anti-rabbit Ig antibody, respectively (both from Dianova, Hamburg, Germany). The slides were washed and coverslipped using carbonate-buffered glycerol, pH 8.6, and evaluated using a BX60 microscope in epifluorescence mode with an appropriate filter set for Cy3. From 5 cross sections per animal per tracheal region, the amount of PGP-immunoreactive and villin-immunoreactive cells were counted, respectively, and normalized to the average diameter of the cervical and thoracic part of the WT animals.

For immunohistochemistry of M2R, mouse trachea from WT and $M2R^{-/-}$ animals were dissected, shock-frozen in melting isopentane and cut at 10 μm thickness. Sections were fixed for 30 min in Zamboni's fixative [24] and then washed repeatedly in 0.1 M PB. Sections were covered for 1 h with PBS containing 10 % normal donkey serum, 0.1 % bovine serum albumin, and 0.5 % Tween 20 followed by incubation with rabbit anti-M2R antibody (1:500, Chemicon, Boronia, Australia). Then, the sections were washed in PBS and covered for 1 h with Cy3-conjugated donkey anti-rabbit Ig antibody (1:1000, Jackson, Baltimore, USA). For multiple-labeling immunofluorescence experiments, the sections were incubated overnight with M2R antibody in combination with a monoclonal FITC-labeled mouse anti-α-smooth muscle actin antibody (1:400, clone 1A4, Sigma, Castle Hill, Australia) and in some experiments with a rat anti-CD31 antibody (1:500, clone MEC 13.3, BD Pharmingen, North Ryde, Australia), washed and covered with Cy3-conjugated donkey anti-rabbit IgG antibody and, if applicable, with Cy5-conjugated donkey anti-rat IgG (1:25, Jackson). After incubation with the secondary reagents, the slides were washed in PBS and coverslipped in carbonate-buffered glycerol at pH 8.6. The slides were evaluated by sequential scanning using a confocal laser scanning microscope (TCS SP5, Leica, Bensheim, Germany).

Measurement of particle transport speed

Mice were killed by inhalation of isoflurane (Baxter, Unterschleissheim, Germany). The thorax was opened and the submandibular gland and the infrahyoid muscles were removed. The trachea was cut caudally to the larynx and cranially to the bifurcation. Then, the trachea was removed and transferred to a Delta T culture dish (Bioptechs, Butler, PA, USA) whose glass bottom was covered with a thin layer of Sylgard polymer (Dow Corning, Wiesbaden, Germany) and that was filled with 2 ml cold Hepes-Ringer solution. Surrounding connective tissue was removed, and the trachea was oriented with the m. trachealis facing upward and fixed with two insect needles. The m. trachealis was cut open using Vannas-Tübingen spring scissors (FST, Heidelberg, Germany). Then, the preparation was gently rinsed with Hepes-Ringer solution to remove mucus followed by exchange with 1.5 ml fresh warm buffer submerging the trachea. The culture dish was transferred to the Delta T Stage holder 30–40 min after the animal's death and was held constant at 30°C. Imaging was done with a Till Vision imaging system (Till Photonics, Gräfelfing, Germany) based on a BX50 WI fixed-stage microscope (Olympus, Hamburg, Germany) equipped with an Imago CCD camera with 1280×960 pixels (Till Photonics).

Prior to measurements, approximately 500,000 polysterene beads of a diameter of 4.5 μm (Dynabeads, Dynal Biotech GmbH, Hamburg, Germany) were added to the buffer solution. Then, the epithelial surface of the trachea was imaged in bright field mode using an UMPLFL20xW/0.50 water immersion objective (Olympus). Muscarine (10^{-4} M, Sigma),

ATP (10-4 M, Sigma) and atropine (10-6 M, Sigma) were added to the dish and were dispersed by gentle pipetting. Polysterene beads were readily identified by their brownish color. An area between two cartilages was chosen for imaging to prevent large differences in image brightness. For each time point 200 images (640×480 pixels; 2×2 binning, 12 bit) were taken with an exposure time of 20 ms at a frame rate of 11.76 images/s.

To determine the track and the speed of individual particles, the following image processing was performed: Non-moving objects in the images were eliminated by subtracting an average image of the 200 images of an individual series from each picture of the series on a pixel-by-pixel basis. If the value of a subtraction got negative, the absolute value was taken. Through this procedure, the image of the formerly darker dynabeads became bright. Then, a copy of this series was changed to a binary picture by a thresholding procedure so that the Dynabeads were set to bright and the background was set to dark. The original film was reduced from 12 bit to 8 bit greyscale and both series were used to track the Dynabeads by an automatic tracking procedure using the TILLvisTRAC software (Till Photonics). Only tracks that were measured over a length of at least 10 frames were included in further calculations.

Measurement of CBF

To measure CBF the trachea was prepared as described for measuring particle transport speed and the same microscope setup was used. An area of the tracheal surface was imaged with an UMPLFL40xW/0.8 water immersion objective (Olympus) and imaging was performed with a high speed EHDcmos1.3 camera (EHD imaging GmbH, Damme, Germany).

One thousand images (640×480 pixels) were taken at a frame rate of 105 images/s. To calculate CBF, the mean gray value of a small area over ciliated cells was determined for each image in the time series. In each imaging series, 10 ciliated cells were evaluated. CBF was determined by resolving the dominating frequency by fast Fourier transformation using AutoSignal 1.7 (Seasolve, Framingham, Ma, USA). For control, areas of the same size were examined in non-ciliated cells. No dominating frequency was present in these control experiments.

Statistical analysis

To compare two experimental conditions and their controls, all groups of the experiment were compared by the Kruskal-Wallis test. If the resulting p was < 0.05, the knockout groups were compared to the WT group using Mann-Whitney tests. The comparison was rated significant if $p < 0.05$.

If time points within a group were examined, all time points were compared by the Friedman Test. If the resulting p was < 0.05 comparison between time points was performed using Wilcoxon Tests. The comparison was rated significant if $p < 0.05$

Results

Expression of MR subtypes in the tracheal epithelium

To identify the MR subtypes that are expressed in tracheal epithelial cells, we analyzed abraded tracheal epithelium of WT mice for the expression of M1-M5R mRNA. We readily identified M1R and M3R mRNA (mean ΔCT for M1R = 7.73, mean ΔCT for M3R = 6.49 as compared to β2-microglobulin mRNA) but not mRNA coding for M2R. Although PCR products for the M4R and the M5R were detectable, the expression levels were too low for

reliable quantification (mean ΔCT for M4R = 13.82, M5R = 12.95, nonspecific PCR products in M2R RT-PCR reached cycle threshold at ΔCT = 12.61).

Immunohistochemistry confirmed the lack of M2R in the mouse tracheal epithelium at the protein level (Figure 1 A–C). M2R-immunoreactivity was not detectable in tracheal airway epithelial cells whereas the antibody readily detected M2R in the tracheal smooth muscle as shown by double-labeling with an α-smooth muscle actin-antibody (Figure 1 D–F). Immunoreactivity for M2R was found in nerve fibers around arteries but was not detected in nerve fibers in the epithelium or in the underlying lamina propria (Figure 1). The M2R-immunoreactivity of these structures was specific since it was absent in sections from $M2R^{-/-}$ mice. Staining of pericyte-like cells in the lamina propria that surrounded CD31-immunoreactive microvascular endothelial cells was non-specific as judged by its presence in sections from $M2R^{-/-}$ animals (Figure S1 in Supplemental Material).

When compared to WT mice, $M1R^{-/-}$ mice exhibited a reduction of M3R mRNA expression (ΔΔCT=1.01, p=0.016). In $M3R^{-/-}$ mice, a reduced amount of M1R mRNA (ΔΔCT=2.37, p=0.008) was detected. In $M2/3R^{-/-}$ mice we did not find a statistically significant change in mRNA expression of M1R mRNA (ΔΔCT=1.47, p=0.095). Expression of M5R and M4R mRNA remained low in all examined knockout lines.

Particle transport speed in WT and MR deficient mice

In WT mice, muscarine (10^{-4} M) induced an increase in particle transport speed (PTS) from 43.5±2.7 (mean±S.E.M) immediately before application of muscarine to 92.0±7.0 μm/s 8 min after drug administration (p=0.002) (Figure 2 A). Subsequent stimulation with ATP (10^{-4} M) resulted in a PTS of 101.3±6.7 μm/s 3 min after application (Figure 2 A, see Supplemental movie 1). This further increase was not statistically significant (p=0.071) In $M3R^{-/-}$ mice, basal PTS was reduced and muscarine had no effect on PTS (p=0.81; Figure 2 A). ATP increased PTS in $M3R^{-/-}$ mice (p=0.002), but the PTS was markedly lower than in WT mice (49.0±8.0 vs. 101.3±6.7 μm/s in WT) (Figure 2 A, see Supplemental movie 2). In $MR1^{-/-}$ mice, muscarine resulted in an increase in PTS from 42.0±4.1 μm/s to 106.6±5.7 μm/s (p=0.02, 8 min after administration) that was not statistically different from that observed in WT animals. Additional application of ATP resulted in a PTS of 107.1±6.0 μm/s (not statistically significant as compared to muscarine alone, p=0.75) which was not significantly different from ATP-stimulated PTS in WT animals.

In $M2R^{-/-}$ mice, addition of muscarine increased PTS comparable to WT level (111.9±11.1 μm/s, p=0.15). In contrast to WT and $M1R^{-/-}$ mice, PTS was further increased by addition of ATP (126.8±10.7 μm/s, p=0.02) (Figure 2 A).

To evaluate if differences in absolute speed were due to differences in basal speed, the value of the 15 min time point was subtracted from each curve from all other time points of the curve (Figure 2 B). Using this approach, the PTS in $M3R^{-/-}$ mice after application of muscarine followed by ATP was still statistically lower than in the other three examined mouse strains (P=0.006). Furthermore, the relative PTS after application of muscarine and ATP in $M2R^{-/-}$ mice as compared to WT mice was statistically significant (p=0.01)

Reduced PTS coincides with reduced CBF in $M3R^{-/-}$ mice

The CBF was determined at the beginning of the experiment, immediately before addition of muscarine, 8 min after addition of muscarine, and 3 min after addition of ATP. These time points correspond with the time points chosen for statistical comparisons of the PTS in previous experiments. During the first 15 min we observed a decrease in CBF in WT as well as in $M1R^{-/-}$, in $M2R^{-/-}$ and in $M3R^{-/-}$ mice (p<0.001 for each strain).

Strikingly, muscarine failed to induce an increase in mean CBF in $M3R^{-/-}$ mice and CBF was even reduced (7.70±0.46 vs 7.40±0.75 Hz, mean±S.E.M. p=0.049). In contrast, WT (11.90±0.63 vs. 20.83±0.80 Hz, p<0.001), $M1R^{-/-}$ (9.80±0.36 19.80±0.67 Hz, p<0.001) and $M2R^{-/-}$ (7.78±0.40 vs.19.63±0.88 Hz) mice responded to muscarine with an increase in CBF.

In all strains, ATP evoked a further, statistically significant increase in CBF in all strains examined (p<0.001). The ATP-induced increase in CBF was substantially smaller in $M3R^{-/-}$ (17.78±1.28 Hz) than in $M1R^{-/-}$ (22.10±0.76 Hz), $M2R^{-/-}$ (23.9±0.77 Hz) and WT mice (29.9±0.77 Hz). Taken together, these data indicate that a lack of increase in CBF can explain the lack of increase in PTS in $M3R^{-/-}$ mice after muscarine application and can partially explain the reduced PTS after additional application of ATP.

To compare the changes in CBF with changes in PTS we calculated the relative increase in CBF by subtracting the value of the 15 min time point and superimposed the data over the curves shown in Figure 2 B (see Figure 2 C). The changes in CBF correlate with changes in PTS although they cannot explain all differences in PTS (e.g. changes in PTS vs. CBF after application of ATP) indicating that additional mechanisms that influence PTS are present.

Role of M4R and M5R in PTS

Neither $M4R^{-/-}$ nor $M5R^{-/-}$ mice differed significantly from WT mice in PTS and its responses to muscarine and ATP (Figure 3).

Relative frequencies of epithelial cell types and morphology do not explain differences in PTS of MR mutant mice

Since differences in the relative frequency of ciliated cells might explain the observed differences in PTS, we quantified the relative frequencies of ciliated cells, non-ciliated cells and basal cells in WT, $M1R^{-/-}$, $M2R^{-/-}$, and $M3R^{-/-}$ mice in the laryngeal and the thoracic part of the trachea (Figure S2 in Supplemental Material). It was previously noted in rats that the relative frequency of ciliated cells is lower in the epithelium overlying the cartilage as compared to areas overlying the ligament or the m. trachealis [25]. Therefore, these areas were assessed separately. As in the rat, we noted a significantly reduced frequency of ciliated cells overlying the cartilage (Table S1 in Supplemental Material). In neither part, however, MR deficiency resulted in differences in cell type composition (see Figure 4 for the epithelium over the ligament of the cervical trachea and Table S1 in Supplemental Material for all data). We also quantified the number of brush cells and neuroendocrine cells by immunolabeling for villin (Figure S3 A–D in Supplemental Material) and PGP 9.5, respectively (Figure S3 E–H in Supplemental Material). We did not find differences in numbers of brush cells in any of the areas examined (Table S2 in Supplemental Material). Neuroendocrine cells were significantly more numerous in the cervical, but not in the thoracic part of the trachea in $M1R^{-/-}$ mice as compared to WT mice (Table S3 in Supplemental Material). To investigate whether changes in ultrastructural morphology accounted for the observed differences in PTS, we examined the tracheal epithelia by electron microscopy. We did not find any significant differences among WT and MR mutant mice in the general structure of the epithelium, the subcellular morphology of ciliated epithelial cells, and of the cilia in particular (Figure 5). The morphological findings indicate that neither number nor subcellular structural alteration of ciliated cells contributed to the observed differences in PTS.

Atropine pretreatment rescues the reduced responsiveness to ATP in $M3R^{-/-}$ mice

Since $M2R^{-/-}$ mice exhibited an enhanced PTS response to ATP, we hypothesized that activation of the M2R prior to ATP stimulation might account for the reduced ATP response

in $M3R^{-/-}$ mice. If this were the case, blockade of all MR by atropine should rescue the effect of ATP in $M3R^{-/-}$ mice. Pretreatment with atropine (10^{-6} M) totally blocked the response to muscarine in WT mice (Figure 6 A). In $M3R^{-/-}$ mice, pretreatment with muscarine restored the ATP response indicating that activation of the M2R is responsible for the blunted response to ATP in the absence of M3R.

Additional M2R deficiency rescues PTS increase to ATP in $M3R^{-/-}$ mice

To validate the inhibitory role of the M2R in $M3R^{-/-}$ mice, we assessed mice deficient for both the M2R and the M3R subtype ($M2/3R^{-/-}$) and their corresponding WT ($M2/3R^{+/+}$) mice for differences in PTS. In line with the hypothesis that the M2R is responsible for the slower PTS in $M3R^{-/-}$ mice, the ATP-induced PTS in $M2/3R^{-/-}$ mice was indistinguishable from that in WT mice (Figure 7). The reactivity to muscarine was partially restored (62.3±5.3 μm/s vs. 104.3±7.5 μm/s in WT) (Figure 7), indicating that inactivation of the M2R not only restores the response to ATP but also unmasks stimulatory effects of other (most likely the M1R) muscarinic receptors.

Discussion

We used six different knockout strains to clarify the role of MR subtypes in the epithelial transport of particles in the trachea. Subtypes M1R, M2R, and M3R, but not M4R and M5R, are substantially involved in the regulation of particle transport.

We determined the function of these receptors using the acutely removed and submerged mouse trachea and focused on particle transport speed for the following reasons. The trachea contains different components such as nerve fibers and/or cells of the immune system that are likely to influence the function of ciliated cells in vivo but would be lost or are not present during long term culture or in isolated cell models. Furthermore, since we could not rule out changes in epithelial morphology, composition, as well as other factors that influence cilia-driven particle transport, determining ciliary beat frequency alone had the risk to overlook other factors that might influence cilia-driven transport without impairing ciliary beat frequency.

Our results show that the three MR subtypes involved in the regulation of PTS (M1R-M3R) exert their actions via different mechanisms. Deficiency of M3R resulted in a total loss of muscarine-induced increase in PTS. This was due to a total lack of increase in CBF, as suggested by classic pharmacological studies on cultured ovine tracheal and frog esophageal epithelium [1, 5]. The influence of the M3R knockout on PTS and CBF was not confined to muscarine but also resulted in a blunted response to ATP if given after stimulation with muscarine. This effect was due to an activation of the M2R as will be discussed below.

Knockout of the M2R resulted in a small increase in the response to muscarine and ATP indicating that the M2R, when activated, can exhibit an inhibitory role. Since the increase was moderate as compared to WT mice, the M2R does not seem to be a major regulator under normal conditions which explains that this receptor was not previously regarded as important for the regulation of cilia-driven transport. However, our data indicate that this inhibitory role of the M2R can be pronounced if the M3R is not functional. In $M3R^{-/-}$ mice, the effect of muscarine reversed from stimulatory to inhibitory leading to a blunted response to ATP if applied after muscarine. This inhibitory effect of muscarine was prevented by preincubation with atropine indicating that it is indeed mediated by a muscarinic receptor. That this inhibitory receptor is the M2R is indicated by the fact that additional knockout of the M2R in $M3R^{-/-}$ mice also reversed the effect of muscarine from inhibitory in $M3R^{-/-}$ to excitatory in $M2/3R^{-/-}$ and restored full reactivity to ATP. Release of acetylcholine and activation of M2R during the removal of the trachea might also explain the reduced basal

rate that was present in $M3R^{-/-}$ mice although this was not a consistent feature of M3R−/− mice (cf. Figure 5).

Since we found neither M2R mRNA nor M2R protein in epithelial cells, the observed M2R-mediated effects are most likely not caused by an epithelial M2R but have to be mediated by other cell types harboring M2R. In general, identification of the cellular distribution of MRs is hampered by the poor quality of antibodies against MRs [26]. Even with the antibody we used which reliably detected the M2R in smooth muscle cells and some nerve fibers and which did not label these structures in $M2R^{-/-}$ mice, we experienced cross reactivity with an unrelated protein in pericytes. Although this antibody can detect M2R in some cells, we cannot be sure that the antibody detects M2Rs in all cell types in the trachea that express this protein. Lung fibroblasts express functional M2R at least under cell culture conditions [27, 28]. Since fibroblasts are found close to the epithelium in airways, it is possible that they can influence ciliated cells. However, the precise cell type(s) through which M2R exert their inhibitory action on the epithelium remain to be determined.

M1R mRNA is expressed in the airway epithelium as judged by real-time RT-PCR. However, in $M1R^{-/-}$ mice, the reactivity to muscarine regarding PTS and CBF was not different from WT mice. This indicates that the presence of the M3R is sufficient for full reactivity to muscarine, and the M1R is not capable of preserving partial reactivity to muscarine in $M3R^{-/-}$ mice. Since we also detected a decrease in M1R-mRNA in $M3R^{-/-}$ mice, it is possible that a reduced M1R receptor expression contributes to this effect. If the inhibitory M2R was deleted in addition to the M3R in $M2/3R^{-/-}$ mice, we could detect an increase in PTS after application of muscarine.

Since MR have been implicated in regulating the proliferation and differentiation of the airway epithelium [4], we expected changes in the morphology and/or relative cell number of epithelial cells. However, we neither found any differences in the number of ciliated, non-ciliated, basal, and brush cells nor in the morphology of these cells among WT and the various MR mutant mice. We only detected an increased number of neuroendocrine cells in $M1R^{-/-}$ mice which was limited to the cervical part of the trachea.

Despite the observed functional differences in the $MR1^{-/-}$, $MR2^{-/-}$, and $M3R^{-/-}$ mice, we did not detect a profound general effect of MR deficiency on the morphology and cell composition of the tracheal epithelium. This shows that these receptors are not necessary for proper development of the epithelium.

Although one has to keep in mind that results derived from experiments in mice are not necessarily applicable to humans, our data indicate that a functional M1R conserves a partial PTS response to acetylcholine and that activation of M2R can reduce the response to ATP. Since M2R and M3R mediate bronchoconstriction in mice [21], selective targeting of the M2R and the M3R might be sufficient to antagonize cholinergic bronchoconstriction also in humans. Blocking M3R and M2R and sparing the M1R would not compromise anticholinergic bronchodilator efficiency but could reduce negative effects on cilia-driven particle transport. Our results also indicate that muscarinic receptors are dispensable during the formation of the airway epithelium.

Supplementary Material

Refer to Web version on PubMed Central for supplementary material.

Acknowledgments

We thank Prof. Dr. D. Drenckhahn for the kind gift of the villin antibody and S. Wiegand for expert animal breeding. M.K.K received a scholarship from the Deutsche Pneumologische Gesellschaft. P.K. received a young scientist grant from the Fachbereich Medizin der Justus-Liebig-Universität Giessen and a grant from the Medizinische Fakultät der Universität zu Läbeck (A31-2007). The study was supported by the DFG, Excellence Cluster Cardiopulmonary System.

References

1. Salathe M, Lipson EJ, Ivonnet PI, Bookman RJ. Muscarinic signaling in ciliated tracheal epithelial cells: dual effects on Ca2+ and ciliary beating. Am J Physiol. 1997; 272(2 Pt 1):L301–L310. [PubMed: 9124382]
2. Wanner A, Salathe M, O'Riordan TG. Mucociliary clearance in the airways. Am J Respir Crit Care Med. 1996; 154(6 Pt 1):1868–1902. [PubMed: 8970383]
3. Lips KS, Volk C, Schmitt BM, Pfeil U, Arndt P, Miska D, Ermert L, Kummer W, Koepsell H. Polyspecific cation transporters mediate luminal release of acetylcholine from bronchial epithelium. Am J Respir Cell Mol Biol. 2005; 33(1):79–88. [PubMed: 15817714]
4. Wessler IK, Kirkpatrick CJ. The Non-neuronal cholinergic system: an emerging drug target in the airways. Pulm Pharmacol Ther. 2001; 14(6):423–434. [PubMed: 11782122]
5. Zagoory O, Braiman A, Gheber L, Priel Z. Role of calcium and calmodulin in ciliary stimulation induced by acetylcholine. Am J Physiol Cell Physiol. 2001; 280(1):C100–C109. [PubMed: 11121381]
6. Caulfield MP, Birdsall NJ. International Union of Pharmacology. XVII. Classification of muscarinic acetylcholine receptors. Pharmacol Rev. 1998; 50(2):279–290. [PubMed: 9647869]
7. Nathanson NM. A multiplicity of muscarinic mechanisms: enough signaling pathways to take your breath away. Proc Natl Acad Sci U S A. 2000; 97(12):6245–6247. [PubMed: 10841527]
8. Wess J. Muscarinic acetylcholine receptor knockout mice: novel phenotypes and clinical implications. Annu Rev Pharmacol Toxicol. 2004; 44:423–450. [PubMed: 14744253]
9. Garssen J, Van Loveren H, Gierveld CM, Van der Vliet H, Nijkamp FP. Functional characterization of muscarinic receptors in murine airways. Br J Pharmacol. 1993; 109(1):53–60. [PubMed: 8495246]
10. Hislop AA, Mak JC, Reader JA, Barnes PJ, Haworth SG. Muscarinic receptor subtypes in the porcine lung during postnatal development. Eur J Pharmacol. 1998; 359(2–3):211–221. [PubMed: 9832393]
11. Fryer AD, el-Fakahany EE. Identification of three muscarinic receptor subtypes in rat lung using binding studies with selective antagonists. Life Sci. 1990; 47(7):611–618. [PubMed: 2402185]
12. Mak JC, Baraniuk JN, Barnes PJ. Localization of muscarinic receptor subtype mRNAs in human lung. Am J Respir Cell Mol Biol. 1992; 7(3):344–348. [PubMed: 1520495]
13. Okada SF, Nicholas RA, Kreda SM, Lazarowski ER, Boucher RC. Physiological regulation of ATP release at the apical surface of human airway epithelia. J Biol Chem. 2006; 281(32):22992–23002. [PubMed: 16754672]
14. Winters SL, Davis CW, Boucher RC. Mechanosensitivity of mouse tracheal ciliary beat frequency: roles for Ca2+, purinergic signaling, tonicity, and viscosity. Am J Physiol Lung Cell Mol Physiol. 2007; 292(3):614–624.
15. Klapproth H, Reinheimer T, Metzen J, Munch M, Bittinger F, Kirkpatrick CJ, Hohle KD, Schemann M, Racke K, Wessler I. Non-neuronal acetylcholine, a signalling molecule synthezised by surface cells of rat and man. Naunyn Schmiedebergs Arch Pharmacol. 1997; 355(4):515–523. [PubMed: 9109369]
16. Yamada M, Lamping KG, Duttaroy A, Zhang W, Cui Y, Bymaster FP, McKinzie DL, Felder CC, Deng CX, Faraci FM, Wess J. Cholinergic dilation of cerebral blood vessels is abolished in M5 muscarinic acetylcholine receptor knockout mice. Proc Natl Acad Sci U S A. 2001; 98(24):14096–14101. [PubMed: 11707605]

17. Yamada M, Miyakawa T, Duttaroy A, Yamanaka A, Moriguchi T, Makita R, Ogawa M, Chou CJ, Xia B, Crawley JN, Felder CC, Deng CX, Wess J. Mice lacking the M3 muscarinic acetylcholine receptor are hypophagic and lean. Nature. 2001; 410(6825):207–212. [PubMed: 11242080]

18. Fisahn A, Yamada M, Duttaroy A, Gan JW, Deng CX, McBain CJ, Wess J. Muscarinic induction of hippocampal gamma oscillations requires coupling of the M1 receptor to two mixed cation currents. Neuron. 2002; 33(4):615–624. [PubMed: 11856534]

19. Gomeza J, Zhang L, Kostenis E, Felder C, Bymaster F, Brodkin J, Shannon H, Xia B, Deng C, Wess J. Enhancement of D1 dopamine receptor-mediated locomotor stimulation in M4 muscarinic acetylcholine receptor knockout mice. Proc Natl Acad Sci U S A. 1999; 96(18):10483–10488. [PubMed: 10468635]

20. Gomeza J, Shannon H, Kostenis E, Felder C, Zhang L, Brodkin J, Grinberg A, Sheng H, Wess J. Pronounced pharmacologic deficits in M2 muscarinic acetylcholine receptor knockout mice. Proc Natl Acad Sci U S A. 1999; 96(4):1692–1697. [PubMed: 9990086]

21. Struckmann N, Schwering S, Wiegand S, Gschnell A, Yamada M, Kummer W, Wess J, Haberberger RV. Role of muscarinic receptor subtypes in the constriction of peripheral airways: studies on receptor-deficient mice. Mol Pharmacol. 2003; 64(6):1444–1451. [PubMed: 14645675]

22. Forssmann WG, Ito S, Weihe E, Aoki A, Dym M, Fawcett DW. An improved perfusion fixation method for the testis. Anat Rec. 1977; 188(3):307–314. [PubMed: 332010]

23. Drenckhahn D, Hofmann HD, Mannherz HG. Evidence for the association of villin with core filaments and rootlets of intestinal epithelial microvilli. Cell Tissue Res. 1983; 228(2):409–414. [PubMed: 6337719]

24. Stefanini M, De Martino C, Zamboni L. Fixation of ejaculated spermatozoa for electron microscopy. Nature. 1967; 216(111):173–174. [PubMed: 4862079]

25. Oliveira MJ, Pereira AS, Guimaraes L, Grande NR, de Sa CM, Aguas AP. Zonation of ciliated cells on the epithelium of the rat trachea. Lung. 2003; 181(5):275–282. [PubMed: 14705771]

26. Zarghooni S, Wunsch J, Bodenbenner M, Bruggmann D, Grando SA, Schwantes U, Wess J, Kummer W, Lips KS. Expression of muscarinic and nicotinic acetylcholine receptors in the mouse urothelium. Life Sci. 2007; 80(24–25):2308–2313. [PubMed: 17337281]

27. Matthiesen S, Bahulayan A, Kempkens S, Haag S, Fuhrmann M, Stichnote C, Juergens UR, Racke K. Muscarinic receptors mediate stimulation of human lung fibroblast proliferation. Am J Respir Cell Mol Biol. 2006; 35(6):621–627. [PubMed: 16902194]

28. Pieper MP, Chaudhary NI, Park JE. Acetylcholine-induced proliferation of fibroblasts and myofibroblasts in vitro is inhibited by tiotropium bromide. Life Sci. 2007; 80(24–25):2270–2273. [PubMed: 17412366]

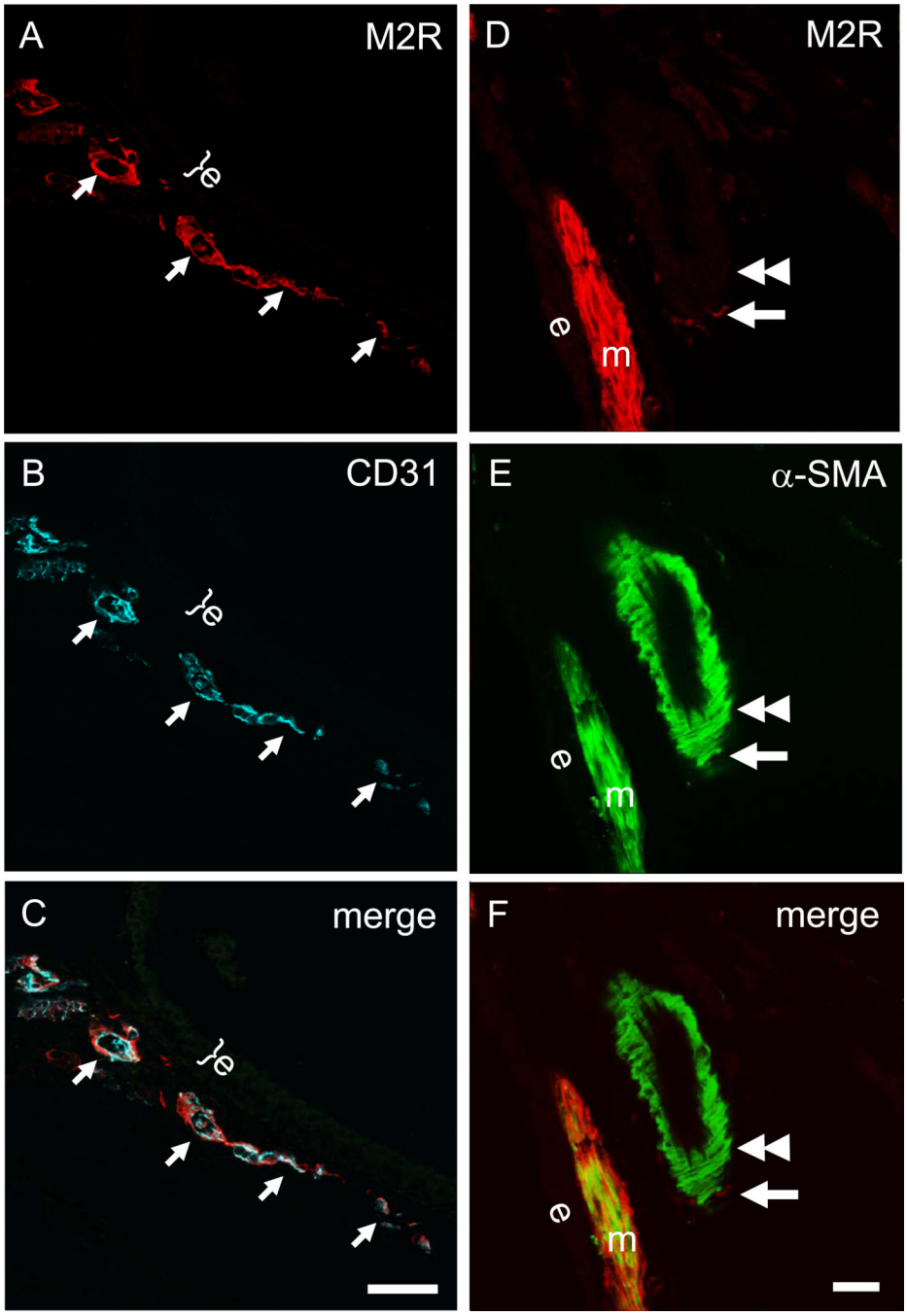

Figure 1. M2R expression in the trachea in WT animals

(A–C) No M2R-immunoreactivity was present in the epithelium (e). Labeling of cells with the morphology resembling pericytes (arrows in A–C) that surrounded CD31-immunoreactive endothelial cells (B) was non-specific as judged by its presence in $M2R^{-/-}$ mice (cf. Figure S1 in Supplemental Material). C. Merge image of A and B. (D–E) Double-labeling immunohistochemistry demonstrated the presence of M2R-immunoreactivity in the membrane of α-smooth muscle actin (α-SMA)-positive airway smooth muscle cells (M) and in nerve fibers close to bronchial arteries (arrows in D–E). The α-SMA-positive vascular smooth muscle (doubled arrowheads) and the airway epithelium (e) showed no M2R-immunoreactivity. Bar in A–C = 50 μm

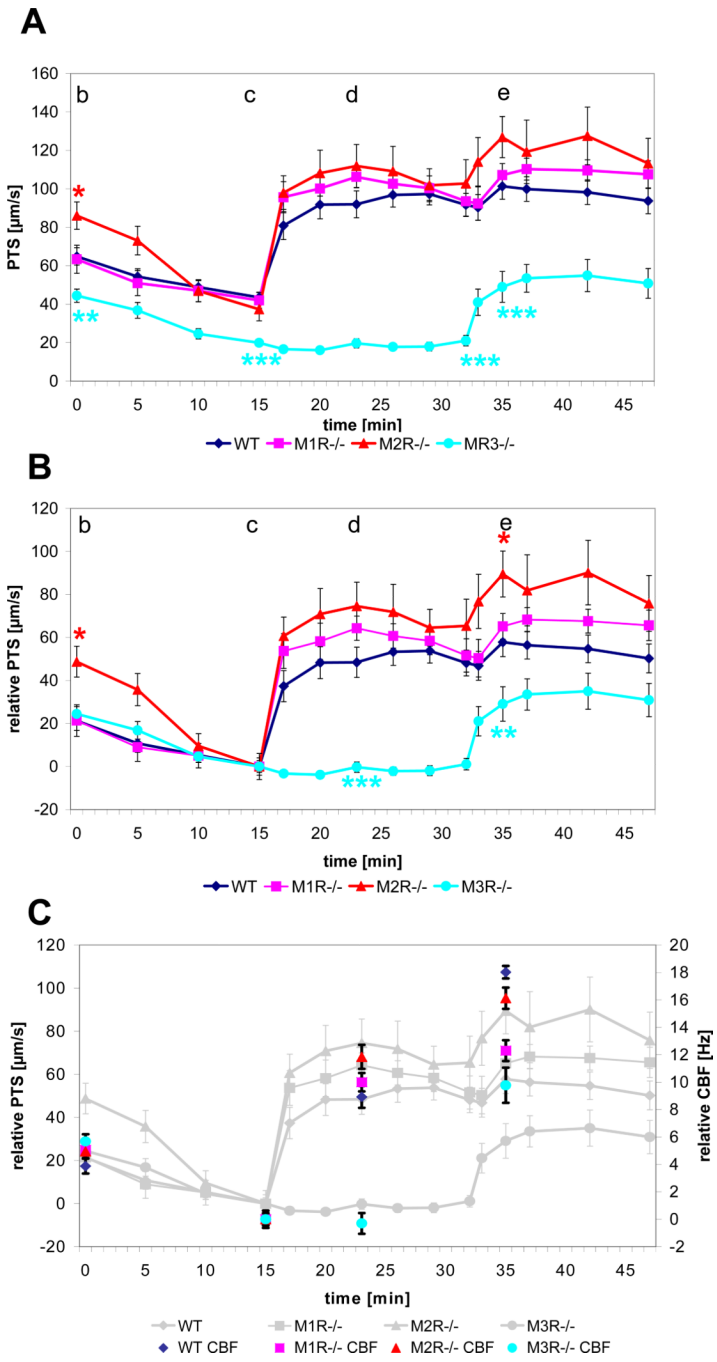

Figure 2. PTS and CBF in response to stimulation of muscarine and ATP in tracheae from WT, M1R$^{-/-}$, M2R$^{-/-}$, and M3R$^{-/-}$ mice

(A) PTS in tracheae from WT, M1R$^{-/-}$, M2R$^{-/-}$, and M3R$^{-/-}$ mice in response to muscarine and ATP. (B) Same experiments as in A but the 15 min value was set to 0 to correct for baseline differences. Data are displayed as mean ± S.E.M., n = 6 for M1R$^{-/-}$ and M2R$^{-/-}$ mice and n = 12 for WT and M3R$^{-/-}$ mice. Statistical analysis of the group differences was performed at (b) the beginning of the experiment, (c) immediately before addition of muscarine, (d) 8 min after addition of muscarine, and (e) 3 min after addition of ATP. Statistical analysis between groups was carried out by Kruskal-Wallis test followed by Mann-Whitney test. * = $p < 0.05$, ** = $p < 0.01$, *** = $p < 0.001$.

(C) Ciliary beat frequency (CBF) corrected for baseline differences is shown from WT, $M1R^{-/-}$, $M2R^{-/-}$, and $M3R^{-/-}$ mice and are superimposed on the graph in B. Data are displayed as mean ± S.E.M., n = 40 cells from 4 animals for each group. CBF was measured at the beginning of the experiment, immediately before addition of muscarine, 8 min after addition of muscarine, and 3 min after addition of ATP. These time points correspond to the time points that were used for the statistical analysis in A and B.

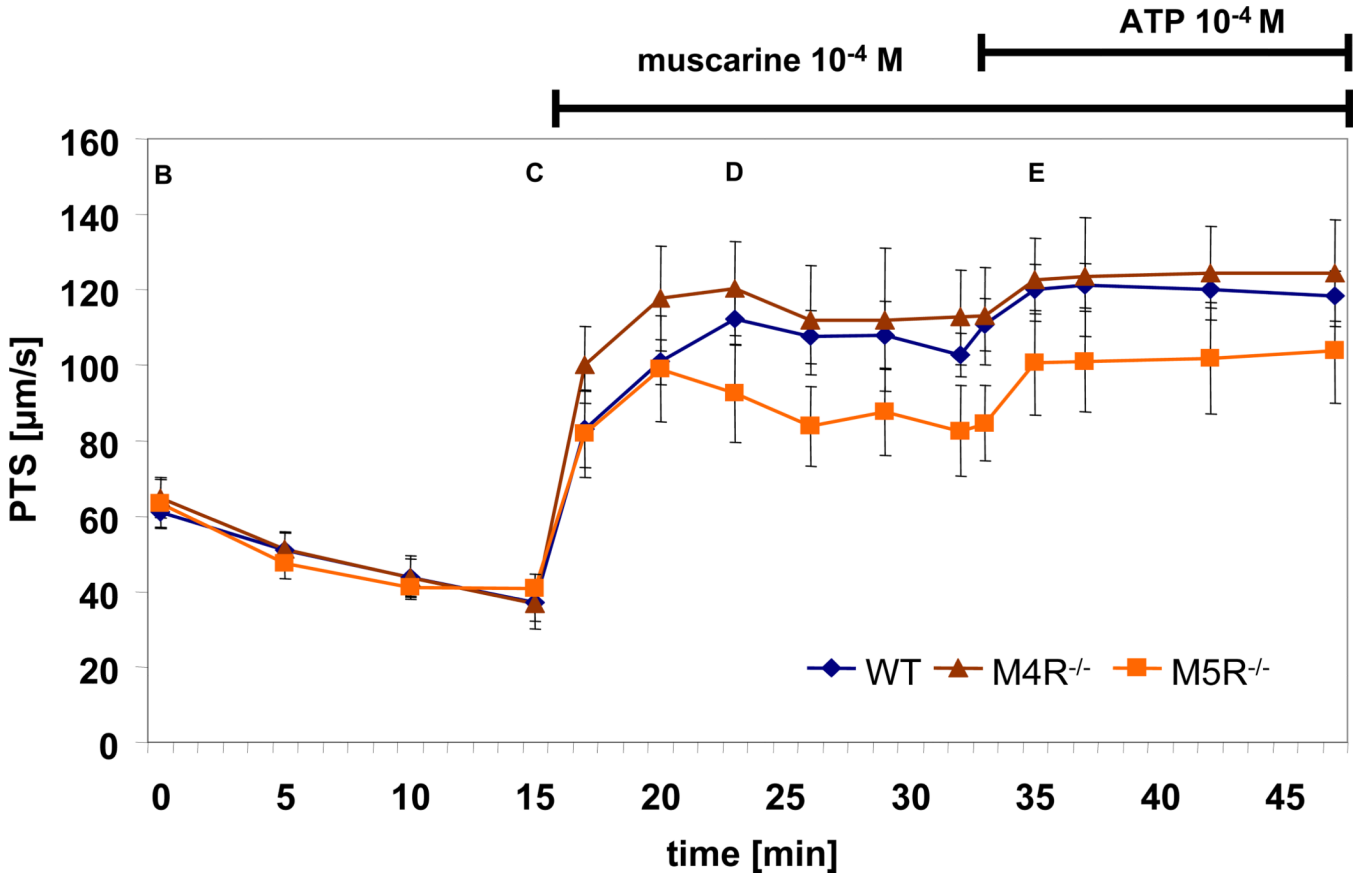

Figure 3. M4R$^{-/-}$ and M5R$^{-/-}$ mice did not differ from WT mice in their PTS response to muscarine and ATP

(A) Data are displayed as mean ± S.E.M., n = 6 for each animal group. Statistical analysis of the group differences at the (b) beginning of the experiment, (c) immediately before addition of muscarine, (d) 8 min after addition of muscarine, and (e) 3 min after addition of ATP. Statistical analysis was carried out by using the Kruskal-Wallis test which showed no statistically significant difference at any of the time points examined.

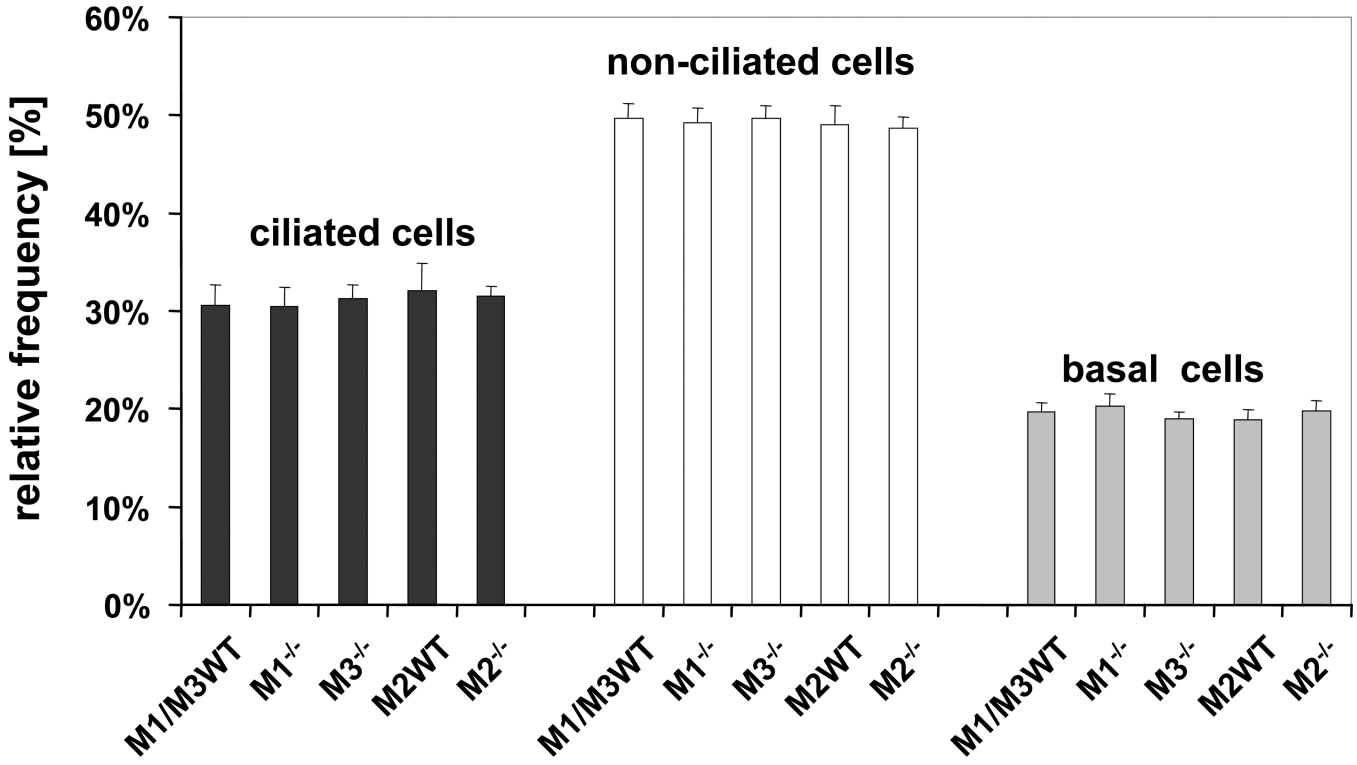

Figure 4. The relative frequency of ciliated, non-ciliated, and basal cells is not changed in WT, $M1R^{-/-}$, $M2R^{-/-}$, and $M3R^{-/-}$ mice over the ligamenta of the cervical trachea

Data are displayed as mean ± S.E.M., n = 5 animals for each group. Statistical analysis was carried out by Kruskal-Wallis test which showed no statistically significant difference. For the complete data please refer to table 2 in the supplemental materials.

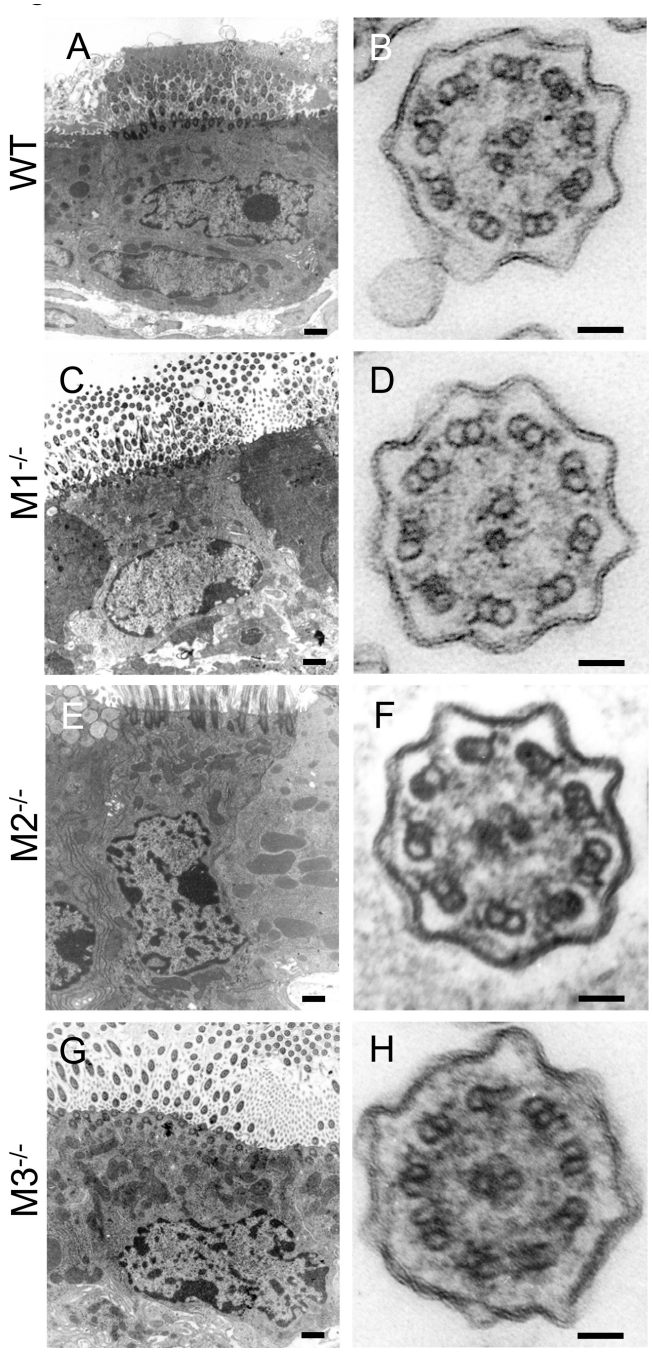

Figure 5. Ultrastructural morphology of cells in the tracheal epithelium of M1R$^{-/-}$, M2R$^{-/-}$, M3R$^{-/-}$ and WT mice

(A, C, E, G) Overview of a ciliated cell. (B, D, F, H) Cilia. Bars = A, C, E, G = 1 μm, B, D, F, H = 0.05 μm

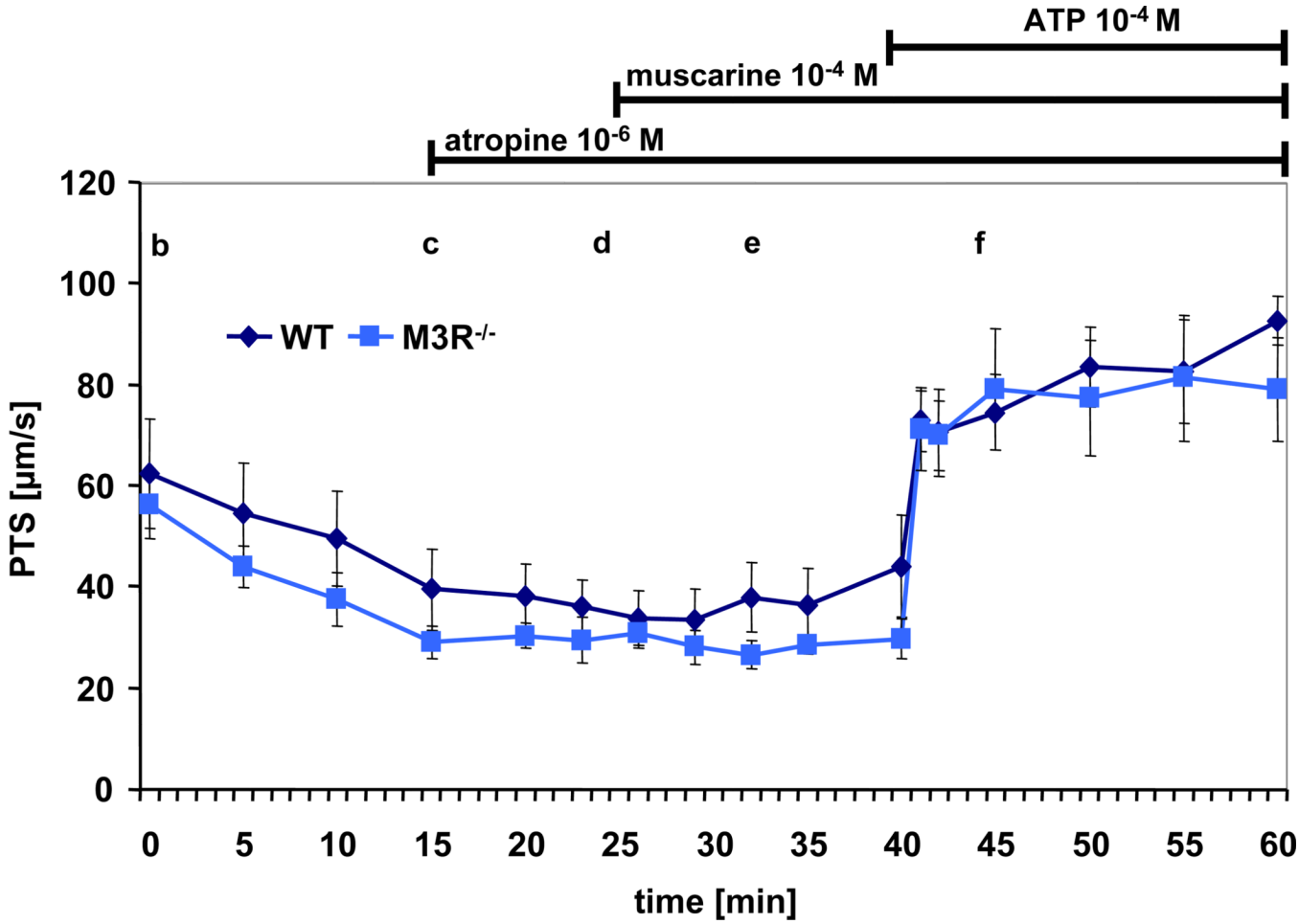

Figure 6. Atropine prevents the blunted PTS response to ATP after application of muscarine in M3R$^{-/-}$ mice

PTS response of M3R$^{-/-}$ mice in comparison to WT mice. Data are displayed as mean ± S.E.M., n = 6 for each animal group. Statistical analysis of the group differences were calculated at the (b) beginning of the experiment, (c) immediately before addition of atropine, (d) 8 min after addition of muscarine, and (e) 3 min after addition of ATP. Statistical analysis was carried out by Kruskal-Wallis test followed by Mann-Whitney test. ** = $p < 0.01$.

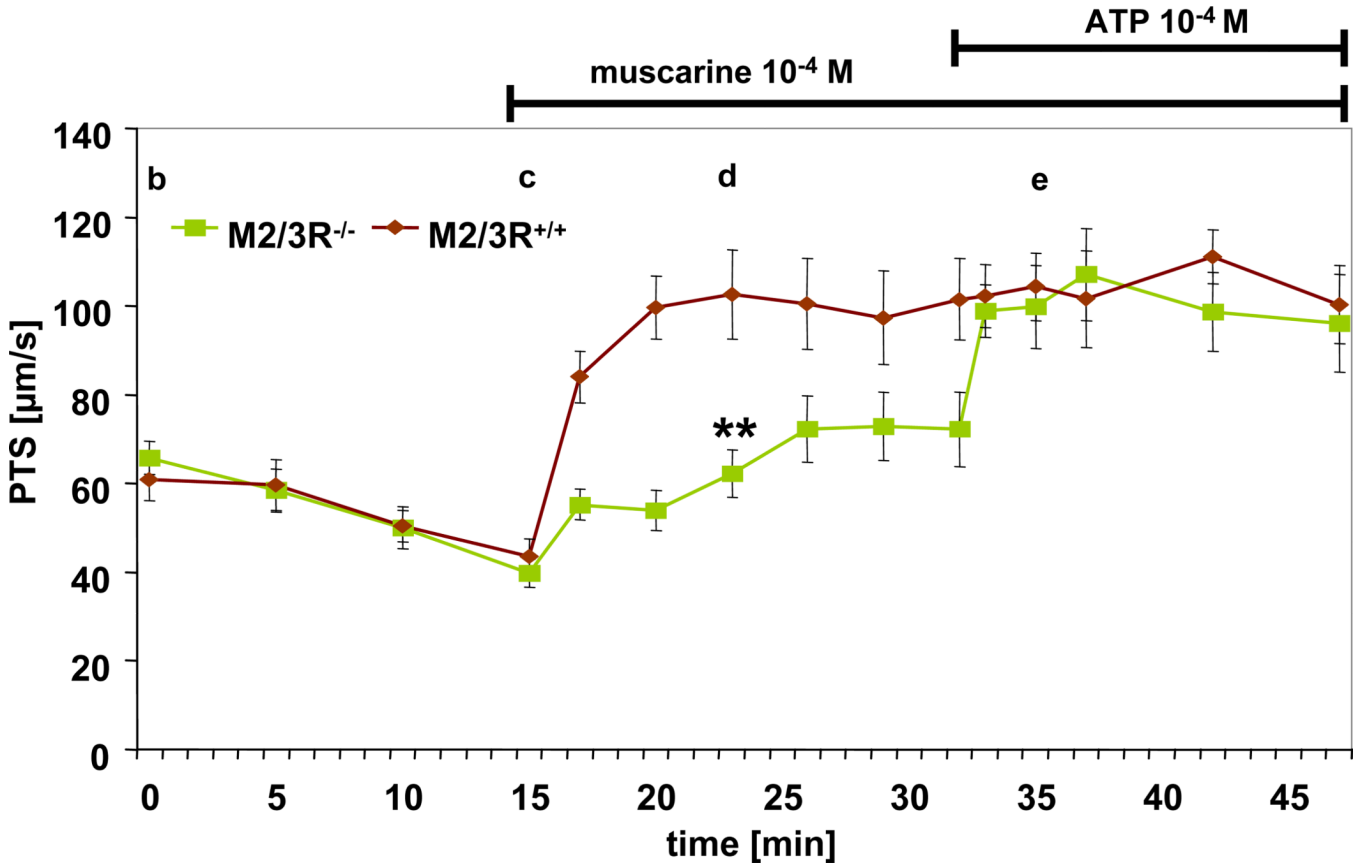

Figure 7. M2/3R$^{-/-}$ mice are responsive to muscarine and show a normal ATP response with respect to PTS

(A) Data are displayed as mean ± S.E.M., n = 6 for each animal group. Statistical analysis of the group differences at the (b) beginning of the experiment, (c) immediately before addition of muscarine, (d) 8 min after addition of muscarine, and (e) 3 min after addition of ATP. Statistical analysis was carried out by Kruskal-Wallis test followed by Mann-Whitney test. * = $p < 0.05$.